SCIENCE CHINA
Chemistry

• ARTICLES •
· SPECIAL TOPIC · Single-Molecule, Single-Particle and Single-Cell Bioimaging

October 2017 Vol.60 No.10: 1305–1309
doi: 10.1007/s11426-016-9028-5

Sub-diffraction-limit cell imaging using a super-resolution microscope with simplified pulse synchronization

Zhaoshuai Gao[1,2], Suhui Deng[1,3], Jiang Li[1], Kun Wang[1], Jiajun Li[1*], Lihua Wang[1] & Chunhai Fan[1]

[1]*Division of Physical Biology & Bioimaging Center, Shanghai Synchrotron Radiation Facility; CAS Key Laboratory of Interfacial Physics and Technology; Shanghai Institute of Applied Physics, Chinese Academy of Sciences, Shanghai 201800, China*
[2]*University of Chinese Academy of Sciences, Beijing 100049, China*
[3]*School of Information Engineering, Nanchang University, Nanchang 330031, China*

Received November 16, 2016; accepted February 27, 2017; published online April 27, 2017

Stimulated emission depletion (STED) microscope is one of the most prominent super-resolution bio-imaging instruments, which holds great promise for ultrahigh-resolution imaging of cells. To construct a STED microscope, it is challenging to realize temporal synchronization between the excitation pulses and the depletion pulses. In this study, we present a simple and low-cost method to achieve pulse synchronization by using a condensed fluorescent dye as a depletion indicator. By using this method, almost all the confocal microscopes can be upgraded to a STED system without losing its original functions. After the pulse synchronization, our STED system achieved sub-100-nm resolution for fluorescent nanospheres and single-cell imaging.

fluorescence microscope, far field super-resolution, stimulated emission depletion (STED) microscope, pulse synchronization

Citation: Gao Z, Deng S, Li J, Wang K, Li J, Wang L, Fan C. Sub-diffraction-limit cell imaging using a super-resolution microscope with simplified pulse synchronization. *Sci China Chem*, 2017, 60: 1305–1309, doi: 10.1007/s11426-016-9028-5

1 Introduction

It has been over millions of years that biosystems are controlled by nanoscaled processes [1,2] and structures [3]. To understand what happens inside a single cell, resolution of the microscope is critical. Since the scales of the cell structures and organelles, e.g., actin [4–6], microtubule [7] and centrosome [8,9] are usually smaller than the optical diffraction limit, traditional optical microscopes can hardly meet the resolution requirement. Therefore scientists are forced to use non-optical [10] or ultra-short electromagnetic wavelength microscopes such as atomic force microscope (AFM) [11], electron microscope (EM) [12,13], and X-ray microscope (XM) [14–16]. The first two instruments are sample invasive and both are short of *in-vivo* imaging capability. The XM could have all the benefits of a fluorescence microscope but this technique is still in the very early research stage [17]. Therefore non-invasive super resolution optical microscope is irreplaceable in nanobio imaging area.

For a microscope, resolution, with no doubt, is one of the most important features. The well-known diffraction limit describes the resolution of any optical system as in the equation below [18–21].

$$d = \frac{0.61\lambda}{n\sin\theta} \quad (1)$$

In the case of fluorescence microscope, the λ defines the wavelength, and the $n\sin\theta$ is the numerical aperture (NA) of the microscope objective. Since the fluorescence emission is usually in the visible spectrum and the highest objective NA can reach 1.4, the resolution of a traditional fluorescence

*Corresponding author (email: jiajunli@sinap.ac.cn)

microscope is around 200 nm [22–24]. During the past two decades, new optical microscope techniques have completely broken the diffraction limit [25–27]. In 1994, Hell *et al*. [28] first proposed to use an extra laser beam to deplete part of the effective fluorescence point spread function (PSF). This idea was implemented in 2000 [29], and it was the first time the optical microscope realized the sub diffraction limit imaging. The principle of the stimulated emission depletion (STED) microscope is to utilize the stimulation emission of light to turn part of the fluorescent molecules into the dark state [30,31].

In a typical STED setup, an extra donut shape depletion beam needs to be spatially overlapped on the excitation beam and their pulses must be temporally synchronized [32,33]. In order to achieve the optimized efficiency, the depletion pulses needed to arrive about few hundreds pico second later than the excitation pulses depending on the excitation wavelength and this is called pulse synchronization [34]. For convenience, continuous wave (CW) STED microscope can be constructed to avoid the complicated pulse synchronization [35–38]. Though the CW STED has a comparable resolution to a common pulse laser STED microscope, it requires an extremely high intensity depletion beam to compete the fluorescence spontaneous emission, which could cause serious damage to the sample [39–41]. In this study, we present a facile method to synchronize the excitation pulses and depletion pulses by using a concentrated fluorescent dye as signal generator to monitor the depletion rate. By doing that, there is no complicated calculation required and the depletion efficiency can be observed in real time.

2 Experimental

In this study, a partially custom-made STED microscope was built on a Leica SP5 confocal microscope system as shown in Figure 1.

A supercontinuum laser (Fianium, SC-450-HE-PP, UK) was used as the illumination and the depletion source of the microscope [42–44]. The broad spectrum (450–2200 nm) laser was separated into two equal intensity beams with perpendicular linear polarization by using a polarization beam splitter (Thorlabs, PBS121, USA). Both beams contain pulses at a rate of 1 MHz and with 350 ps temporal width [34]. The excitation beam was filtered out by a band pass filter (Semrock, FF02-482/18-25; or Semrock, FF01-561/14-25, USA) followed by a spatial filter. A set of mirrors on a linear stage was used as a time delay system for synchronization. The depletion beam was filtered out by a 650 nm band pass filter and also followed by a spatial filter. An electric beam shutter (Thorlabs, SH05, USA) was used to open and close the depletion beam periodically. Then the depletion beam was recombined with the excitation beam by a dichroic mirror (Semrock, FF580-FDI01-25X36, USA). A λ/4 waveplate (Thorlabs, AQWP05M-600, USA) was used to convert both beams into circular polarization.

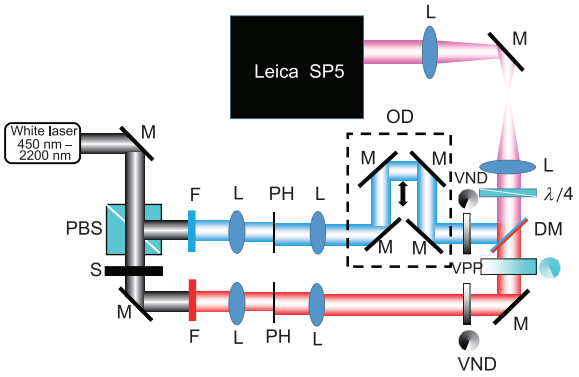

Figure 1 Schematic of the partially custom made STED microscope. M: mirror; PBS: polarization beam splitter; S: electric beam shutter; F: bandpass filter; L: lens; PH: pinhole; VND: variable ND filter; VPP: vortex phase plate; DM: dichroic mirror; λ/4: quarter wave plate; OD: optical delay (color online).

3 Results and discussion

In pulse synchronization, the recombined beam was first superpositioned with the Leica 592 nm laser source by using a custom made multi-wavelenth dichroic mirror (Chroma Technology, ZT405/488/561/647 rpc, φ 10 mm, USA). The PSF of all the beams were carefully overlapped in x, y and z directions by observing the 80 nm golden nanoparticles [45] in reflection mode as shown in Figure 2.

After the beams were spatially superpositioned, they need to be temporally synchronized. A concentrated Atto 565 fluorophore solution (C=3.27 mM) was used as signal generator. Such high concentration fluorescent solution could be exposed under the excitation illumination for a long time (>60 min) with neglectable photobleaching. During the imaging process the electric shutter switched the depletion beam periodically on and off. Due to the stimulation phenomenon a series of bright and dark images were recorded, which indicated the shutter movement as shown in Figure 3(b). Then the average intensity was calculated and plotted as shown in Figure 3(d).

By dividing the "dark" image (Figure 3(c), after depletion) integral intensity s0 to the "bright" image (Figure 3(c), before depletion) integral intensity s1, the remaining fluorescent intensity (RFI) can be calculated. The linear stage controlled optical delay system can easily move in mm scale. After every 5 mm movement (17 ps optical delay), the RFI was recorded and plotted as shown in Figure 4. From the figure, it is easy to see that the most efficient depletion rate happens when the delay system introduced a 35 mm extra optical path which equals to approximately 120 ps delay temporally and

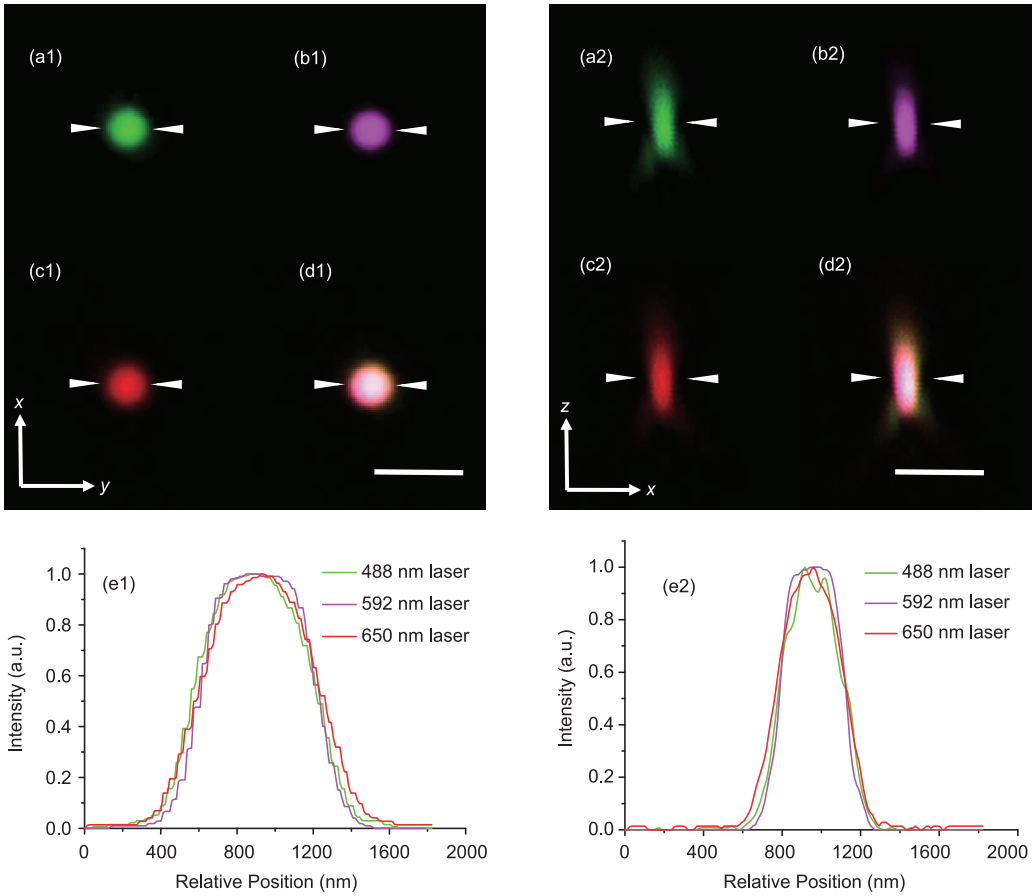

Figure 2 (a1, a2) The PSF of STED excitation beam 482 nm; (b1, b2) SP5's 592 nm laser; (c1, c2) STED depletion beam 650 nm in lateral (left) and longitudinal (right) directions; (d1, d2) overlapped PSF of the 488, 592 and 650 nm; (e1, e2) intensity profile of *x*-*y* and *x*-*z* plane through the triangle tip. Scale bar: 500 nm (color online).

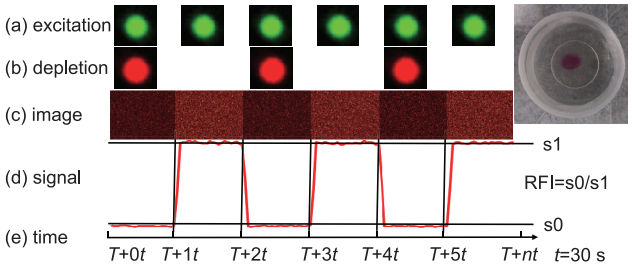

Figure 3 To observe the depletion rate, excitation beam was constantly illuminated (a), and the depletion beam was switched off periodically (b). It caused the microscope gave a periodic "bright" and "dark" image set (c). By calculating the average signal difference (d) based on time (e), we are able to directly view the change of depletion rate (color online).

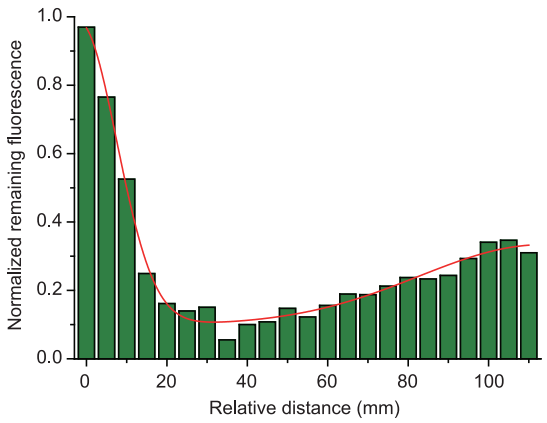

Figure 4 The depletion rate variance was plotted by changing the length of the optical delay path (color online).

this depletion curve highly matches the results of Paolo Bianchini published in 2012 [46]. The same synchronization procedure can also be used to synchronize the 482 nm (excitation)/650 nm (depletion) pulses.

After the pulse synchronization, a 0-2π vortex phase plate (RPC Photonics, VPP1a) was placed into the depletion beam before the $\lambda/4$ phase plate at the conjugated point respect to the objective rear focal plane to create the donut shape PSF as shown in Figure 5. The optical path different introduced by the vortex phase plate can be negligible as the gradient of the curve is very small at the bottom. The intensity profile in Figure 5(g) revealed the intensity of the donut center was very close to background.

To confirm the performance of our ultra-simple optical delay method, we prepared a complex which contained 40 nm

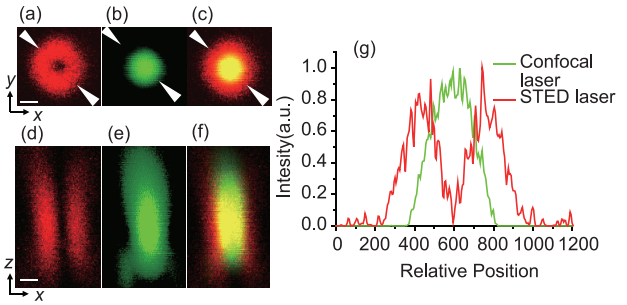

Figure 5 The PSF of STED excitation beam (green), depletion beam (red) in lateral (a, b, c) and longitudinal (d, e, f) directions; (g) the intensity plot of the donut circle and excitation in its lateral direction (c) which indicated the darkness of its zero intensity center. Scale bar: 200 nm (color online).

streptavidin conjugated nanosphere with biotin labeled Atto 488. Although this approach of labeling is very easy to cause sample aggregation, the fluorophore can be easily replaced for different wavelength resolution test. The fluorescent nanospheres is imaged by using a conventional confocal microscope and our partially customized STED microscope. In both microscopes the wavelength of the excitation beams were set at 482 nm and the intensities were 40 μW at the objective back focal plane. In STED microscope the depletion beam was 650 nm and the intensity was 2 mW at the objective back focal plane. The optical delay system introduced an extra 35 mm optical path in the depletion beam and the pixel dwell time was about 100 μs. By comparing the size of the nanospheres in Figure 6(a) and (b), we were able to observe the size reduction. The Figure 6(e) plotted the intensity across a single nanosphere in Figure 6(c) and (d). The intensity profile indicated the FWHM of the nanosphere imaged by the STED microscope was about 69 nm fitted by Lorentzian function which was more than 3 folds smaller than the one taken by the conventional confocal microscope.

To prove the system could also work with biological samples, the HeLa cell tubulin was immuno-staining by Atto 565 fluorophore and used as a sample. The images were taken under the same condition as in the previous experiment except the wavelength of the excitation beam was changed to 561 nm. In Figure 7, the STED images revealed more detail of the cell tubulin distribution. Figure 7(c) and (d) were the zoom in of the white squares in Figure 7 (a) and (b) which further confirmed the resolution enhancement. Figure 7(e) was the intensity plot across a single tubulin fiber and the solid line is the fitting line by Lorentzian function. It showed the FWHM of a single fiber was 80 nm which was more than 2 times thinner than the one taken by the confocal microscope.

4 Conclusions

In this study, we presented a simple and inexpensive method to synchronize the excitation pulse and the depletion pulse for

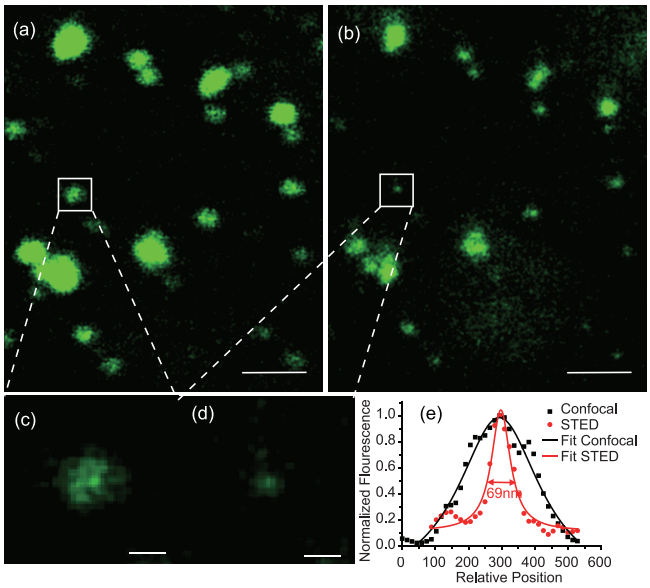

Figure 6 The fluorescent images of 40 nm diameter fluorescent nanospheres taken by confocal microscope (a) and STED microscope (b); (c, d) the zoom of the white squares in (a) and (b); (e) the intensity profile of a single fluorescent nanosphere. Scale bar: (a, b) 1 μm; (c, d) 200 nm (color online).

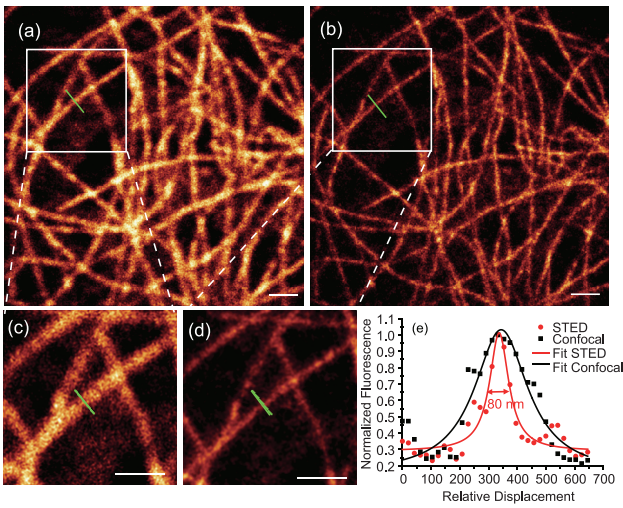

Figure 7 The fluorescent images of HeLa cell tubulin taken by confocal microscope (a) and STED microscope (b); (c, d) the zoom of the white squares in (a) and (b); (e) the intensity profile of a single fibril (along green lines in (c)and (d)). Scale bar 1 μm (color online).

pulsed laser STED microscope. In this method, there is no need of high speed oscilloscope and fast photodiode, which should enable conventional labs to build their own STED system. The real time optical path delay adjustment enables users to directly observe the moment when the maximum depletion happens, therefore no complicated calculation is needed for the length of delay. To prove the performance of this method, we performed both biological and non-biological imaging experiments. Both results confirmed the efficiency of the depletion and the lateral resolution can achieve

69 nm. This method can also be used in constructing time gating STED microscope with a TCSPC card to observe the depletion curve in nanosecond scale.

Acknowledgments This work was supported by the National Natural Science Foundation of China (21227804, 21390414, 61378062, 21505148), National Key Research and Development Program (2016YFA0400902) and the Natural Science Foundation of Shanghai (15ZR1448400, 14ZR1448000).

Conflict of interest The authors declare that they have no conflict of interest.

1 Zhao Y, Chen F, Li Q, Wang L, Fan C. *Chem Rev*, 2015, 115: 12491–12545
2 Zhao Y, Qi L, Chen F, Zhao Y, Fan C. *Biosens Bioelectron*, 2013, 41: 764–770
3 Song S, Qin Y, He Y, Huang Q, Fan C, Chen HY. *Chem Soc Rev*, 2010, 39: 4234–4243
4 Xu K, Zhong G, Zhuang X. *Science*, 2013, 339: 452–456
5 Urban NT, Willig KI, Hell SW, Nägerl UV. *Biophys J*, 2011, 101: 1277–1284
6 D'Este E, Kamin D, Göttfert F, El-Hady A, Hell SW. *Cell Rep*, 2015, 10: 1246–1251
7 Huang F, Sirinakis G, Allgeyer ES, Schroeder LK, Duim WC, Kromann EB, Phan T, Rivera-Molina FE, Myers JR, Irnov I, Lessard M, Zhang Y, Handel MA, Jacobs-Wagner C, Lusk CP, Rothman JE, Toomre D, Booth MJ, Bewersdorf J. *Cell*, 2016, 166: 1028–1040
8 Mennella V, Keszthelyi B, McDonald KL, Chhun B, Kan F, Rogers GC, Huang B, Agard DA. *Nat Cell Biol*, 2012, 14: 1159–1168
9 Lawo S, Hasegan M, Gupta GD, Pelletier L. *Nat Cell Biol*, 2012, 14: 1148–1158
10 Jia S, Chao J, Fan C, Liu H. *Prog Chem*, 2014, 26: 695–705
11 Elie-Caille C, Severin F, Helenius J, Howard J, Muller DJ, Hyman AA. *Curr Biol*, 2007, 17: 1765–1770
12 Viswanathan S, Williams ME, Bloss EB, Stasevich TJ, Speer CM, Nern A, Pfeiffer BD, Hooks BM, Li WP, English BP, Tian T, Henry GL, Macklin JJ, Patel R, Gerfen CR, Zhuang X, Wang Y, Rubin GM, Looger LL. *Nat Meth*, 2015, 12: 568–576
13 de Boer P, Hoogenboom JP, Giepmans BNG. *Nat Meth*, 2015, 12: 503–513
14 Zhu Y, Earnest T, Huang Q, Cai X, Wang Z, Wu Z, Fan C. *Adv Mater*, 2014, 26: 7889–7895
15 Rambo RP, Tainer JA. *Annu Rev Biophys*, 2013, 42: 415–441
16 Tian T, Zhang JC, Lei HZ, Zhu Y, Shi JY, Hu J, Huang Q, Fan CH, Sun YH. *Nucl Sci Tech*, 2015, 3: 102–107
17 Xu H, Li Q, Wang L, He Y, Shi J, Tang B, Fan C. *Chem Soc Rev*, 2014, 43: 2650–2661
18 Hou SG, Liang L, Deng SH, Chen JF, Huang Q, Cheng Y, Fan CH. *Sci China Chem*, 2014, 57: 100–106
19 Ke MT, Nakai Y, Fujimoto S, Takayama R, Yoshida S, Kitajima TS, Sato M, Imai T. *Cell Rep*, 2016, 14: 2718–2732
20 Willets KA. *Phys Chem Chem Phys*, 2013, 15: 5345–5354
21 Lu RW, Wang BQ, Zhang QX, Yao XC. *Biomed Opt Express*, 2013, 4: 1673–1682
22 Abbe E. *Archiv für mikroskopische Anatomie*, 1873, 9: 413–418
23 Nägerl UV, Willig KI, Hein B, Hell SW, Bonhoeffer T. *Proc Natl Acad Sci USA*, 2008, 105: 18982–18987
24 Liu Y, Ding Y, Alonas E, Zhao W, Santangelo PJ, Jin D, Piper JA, Teng J, Ren Q, Xi P. *PLoS ONE*, 2012, 7: e40003
25 Betzig E, Patterson GH, Sougrat R, Lindwasser OW, Olenych S, Bonifacino JS, Davidson MW, Lippincott-Schwartz J, Hess HF. *Science*, 2006, 313: 1642–1645
26 Rust MJ, Bates M, Zhuang X. *Nat Meth*, 2006, 3: 793–796
27 Hess ST, Girirajan TPK, Mason MD. *Biophys J*, 2006, 91: 4258–4272
28 Hell SW, Wichmann J. *Opt Lett*, 1994, 19: 780–782
29 Klar TA, Jakobs S, Dyba M, Egner A, Hell SW. *Proc Natl Acad Sci USA*, 2000, 97: 8206–8210
30 Huang B, Babcock H, Zhuang X. *Cell*, 2010, 143: 1047–1058
31 Wang S, Deng S, Cai X, Hou S, Li J, Z Gao, Li J, Wang L, Fan C. *Sci China Chem*, 2016: 1519–1524
32 Rankin BR, Kellner RR, Hell SW. *Opt Lett*, 2008, 33: 2491–2493
33 Rankin BR, Hell SW. *Opt Express*, 2009, 17: 15679–15684
34 Yu JQ, Yuan JH, Zhang XJ, Liu JL, Fang XH. *Chin Sci Bull*, 2013, 58: 4045–4050
35 Willig KI, Harke B, Medda R, Hell SW. *Nat Meth*, 2007, 4: 915–918
36 Beater S, Holzmeister P, Lalkens B, Tinnefeld P. *Opt Express*, 2015, 23: 8630–8638
37 Moneron G, Medda R, Hein B, Giske A, Westphal V, Hell SW. *Opt Express*, 2010, 18: 1302–1309
38 Du J, Deng S, Hou S, Qiao L, Chen J, Huang Q, Fan C, Cheng Y, Zhao Y. *Chin Opt Lett*, 2014, 12: 0411011
39 Donnert G, Eggeling C, Hell SW. *Nat Meth*, 2007, 4: 81–86
40 Boudreau C, Wee TLE, Duh YRS, Couto MP, Ardakani KH, Brown CM. *Sci Rep*, 2016, 6: 30892
41 Vicidomini G, Moneron G, Han KY, Westphal V, Ta H, Reuss M, Engelhardt J, Eggeling C, Hell SW. *Nat Meth*, 2011, 8: 571–573
42 Wildanger D, Rittweger E, Kastrup L, Hell SW. *Opt Express*, 2008, 16: 9614–9621
43 Chéreau R, Tønnesen J, Nägerl UV. *Methods*, 2015, 88: 57–66
44 Gao F, Zhang Y, Yang H, Xiao Y, Wei T, Chang J. *Optik - Int J Light Electron Optics*, 2016, 127: 6610–6617
45 Osseforth C, Moffitt JR, Schermelleh L, Michaelis J. *Opt Express*, 2014, 22: 7028–7039
46 Galiani S, Harke B, Vicidomini G, Lignani G, Benfenati F, Diaspro A, Bianchini P. *Opt Express*, 2012, 20: 7362–7374